Journal of Catalysis 281 (2011) 325–338

Contents lists available at ScienceDirect

Journal of Catalysis

journal homepage: www.elsevier.com/locate/jcat

Selective poisoning of the direct denitrogenation route in o-propylaniline HDN by DBT on Mo and NiMo/γ-Al_2O_3 sulfide catalysts

Ana Hrabar, Jennifer Hein, Oliver Y. Gutiérrez, Johannes A. Lercher *

Technische Universität München, Department of Chemistry, Catalysis Research Center, Lichtenbergstraße 4, 85747 Garching, Germany

ARTICLE INFO

Article history:
Received 7 March 2011
Revised 12 May 2011
Accepted 14 May 2011
Available online 17 June 2011

Keywords:
Hydrodenitrogenation
o-Propylaniline
Dibenzothiophene
MoS_2/γ-Al_2O_3
NiMoS/γ-Al_2O_3

ABSTRACT

The hydrodenitrogenation of o-propylaniline on MoS_2/γ-Al_2O_3 and NiMoS/γ-Al_2O_3 catalysts proceeds via two parallel routes, i.e., direct denitrogenation (DDN) by C(sp^2)–N bond cleavage to form propylbenzene and hydrogenation (HYD) of the phenyl ring to form propylcyclohexylamine, followed by C(sp^3)–N bond cleavage. Coordinatively unsaturated sites (CUS) at the edges of the sulfide slabs are catalytically active for the DDN. Dibenzothiophene (DBT) decreases the DDN rate, while it is mainly converted via direct desulfurization. Adding Ni to MoS_2 increases the CUS concentration and promotes the HYD but inhibits the DDN, suggesting that Ni cations are not involved in the active sites for DDN route. Catalytically active sites for the HYD route are the sites at the basal plane near the edges of the sulfide slabs (brim sites). The presence of DBT strongly increases the HYD rate on NiMoS/γ-Al_2O_3, increasing the electron density at the brim sites due the electron pair donor properties of DBT and biphenyl.

1. Introduction

As one of the key hydrotreating reactions, hydrodenitrogenation (HDN) on sulfide-based catalysts has been studied extensively, because of its complexity and inhibiting effects on other hydrotreating reactions. Despite these efforts, it is still difficult to unequivocally establish an atomistic picture of the active sites involved in the various elementary steps in HDN [1].

Although basic nitrogen-containing compounds adsorb readily onto the acidic surface of the sulfides and the support, it is not likely that every sorbate will lead to reaction and in turn reactants and products may inhibit certain pathways. Thus, better knowledge of the active sites is expected to lead to a more specific optimization of hydrotreating catalysts. With this in mind, we attempt in the present contribution to specify the sites active for HDN, in particular of o-propylaniline (OPA), a key intermediate in the HDN of quinoline.

MoS_2, which is the basis of most HDN catalysts, is buildup by trigonal sulfur prisms coordinated to Mo, which are, in turn, two-dimensionally bound, forming S–Mo–S sandwiched structures. These slabs exhibit two different active edges, so-called Mo-edge and S-edge. The nano-crystalline MoS_2 slabs are weakly held together by van der Waals interactions along the *c*-axis. The degree of stacking of the S–Mo–S layers depends on the synthesis conditions, metal loading, and surface area of the used support material.

Upon addition of Co and Ni, the Mo cations are substituted at the edge positions of the MoS_2 slabs. This substitution of Mo cations by Co and Ni is believed to be crucial in the creation of new and more active catalytic sites [2,3]. Recent DFT studies show that Co and Ni substitutions are favorable at the S-edge and Mo-edge, respectively [4,5]. Co as a promoter is predominantly located in a tetrahedral coordination, while Ni exists in a square-planar environment and under typical hydrotreating conditions, the equilibrium morphology for CoMoS and NiMoS are close to hexagon and deformed hexagon, respectively [6]. Upon substitution, sulfur vacancies are formed, i.e., coordinatively unsaturated sites (CUS), because the sulfur binding energy decreases in the order MoS_2 > CoMoS > NiMoS [7], thus reducing the equilibrium sulfur coverage and increasing the concentration of accessible metal cations. Electron-rich zones have been identified on the basal plane in model catalysts by high-resolution scanning tunneling microscopy and have been associated with metal-like states [8,9].

While it is considered that the direct removal of sulfur and nitrogen atoms by CUS sites proceeds via a reverse Mars–van Krevelen mechanism (the S or N atom, initially in the molecule, remains in the catalyst surface after the reaction), the sites involved in hydrogenation reactions are less understood. In essence, the hydrogenation involving CUS sites at the edge, sites at the basal plane near the edge (brim sites), and sites that combine both have been proposed [10–12]. The role of the promoter is on the one hand to increase the concentration of sulfur vacancies (CUS, accessible metal cations) and on the other hand to increase the electron density at the brim sites [13]. Both factors may influence the activity and selectivity of the HDN reaction, and we will therefore

* Corresponding author. Fax: +49 89 289 13544.
E-mail address: Johannes.Lercher@ch.tum.de (J.A. Lercher).

0021-9517/$ - see front matter © 2011 Published by Elsevier Inc.
doi:10.1016/j.jcat.2011.05.017

attempt to relate the observed reaction pathways to these two sites or their combination.

The HDN of quinoline [14–21] has been explored frequently over the last decades, because of its bicyclic nature, which allows exploring all elementary HDN steps. The reaction starts with the hydrogenation of the pyridinic ring followed by ring opening via C(sp^3)-N bond cleavage forming OPA, followed by direct nitrogen removal (DDN) or hydrogenation of benzoic ring followed by nitrogen removal either by ammonia elimination or by substitution of NH_2 by -SH and further C–S hydrogenolysis. In order to better understand the critical reaction steps in the overall sequence, this study is focused on the HDN of the key intermediate o-propylaniline. Competitive adsorption of various basic nitrogen-containing intermediates is so avoided ensuring the absence of additional inhibition effects. OPA HDN proceeds via hydrogenation of the aromatic ring and aliphatic C(sp^3)-N bond cleavage (HYD), as well as direct aromatic C(sp^2)-N bond cleavage (DDN).

In this contribution, the HDN of OPA on MoS_2/γ-Al_2O_3 and NiMoS/γ-Al_2O_3 sulfide catalyst is explored. The aim of the paper is to address the impact of Ni on the catalytic properties of MoS_2 and to study the impact of sulfur-containing compounds (using dibenzothiophene) on the catalytic activity and selectivity. Overall, it is aimed to provide evidence for the nature of the active sites responsible for different reaction routes using titration of sites and kinetic measurements.

2. Experimental

2.1. Catalyst preparation

The supported Mo and NiMo oxide catalyst precursors were prepared by incipient wetness impregnation of γ-Al_2O_3. Prior to impregnation, the support was dried at 120 °C and then calcined at 560 °C for 2 h in synthetic air flow. At first, molybdenum was impregnated using an aqueous solution of ammonium heptamolybdate, $(NH_4)_6Mo_7O_{24}{\cdot}4H_2O$ (Aldrich). After impregnation, the catalyst was dried overnight at 120 °C in static air atmosphere and then thermally treated at 500 °C for 4 h (heating rate 1 °C/min) in flowing synthetic air [22]. One part of the prepared Mo catalyst was kept as precursor for kinetic experiments, and the other was used as a support for further nickel impregnation with an aqueous solution of nickel nitrate, $Ni(NO_3)_2{\cdot}6H_2O$ (Aldrich) [23]. After impregnation, the NiMo catalyst was dried and thermally treated as in case of the Mo catalyst.

2.2. Catalyst characterization

2.2.1. Physicochemical properties of the catalyst

The BET surface area and pore size distribution were determined by N_2 adsorption–desorption at −196 °C using a PMI Automated BET Sorptomatic 1900 Series instrument. Prior to the adsorption, the samples were evacuated at 250 °C for 2 h. Elemental analysis was carried out in the Microanalytical Laboratory at the TU München.

2.2.2. X-ray diffraction (XRD)

The crystalline structure of the catalysts was determined by powder X-ray diffraction. XRD patterns were collected with a Philips X'Pert System (Cu Kα radiation, 0.1542 nm), using a nickel K_β-filter and solid-state detector (X'Celerator). The operating conditions were 45 kV/40 mA. The measurements were carried out in a range from 5° to 70° 2θ with a step size of 0.017° and scan time of 115 s per step.

2.2.3. Transmission electron microscopy (TEM)

Sulfided catalysts were ground, suspended in ethanol, and ultrasonically dispersed. Dispersion drops were applied on a copper-carbon grid. Measurements were carried out on transmission electron microscope device JEOL JEM-2011 with an accelerating voltage of 120 keV.

2.2.4. Raman spectroscopy

Raman spectra of oxide precursors and sulfided catalysts were obtained with a Renishaw Raman Spectrometer (Type 1000), equipped with CCD detector and Leica microscope, using 514-nm Ar laser. Prior to the measurements, calibration was done with Si (111) crystal. The wavenumber accuracy was within 1 cm^{-1}. Oxidic catalyst precursors were analyzed under ambient conditions, and therefore, the samples were pressed into self-supported wafers and placed onto a quartz sample holder. The used sulfide catalyst was analyzed using a diode 785-nm laser.

2.2.5. Temperature-programmed sulfidation (TPS)

To study the influence of nickel as a promoter on the sulfidation mechanism, catalyst activation was performed by temperature-programmed reaction/sulfidation (TPS). The oxide precursor (0.1 g) was placed in the flow reactor equipped with a ceramic oven (Horst GmbH). The activation was performed in 10% H_2S in H_2 with a heating rate of 5 °C/min. At 400 °C, the temperature was held isothermally for 1 h. Evolved gases were detected by a mass spectrometer (Balzers QME 200).

2.2.6. NO adsorption

NO adsorption was applied to probe the active sites and average edge dispersion in the supported metal sulfide catalysts, such as unpromoted MoS_2/γ-Al_2O_3 and promoted NiMoS/γ-Al_2O_3. NO adsorption was performed as a flow pulse experiment at room temperature. After activation in 10% H_2S in H_2 at 400 °C, the catalyst was cooled to room temperature in the presence of the sulfiding agent. Then, the catalyst was flushed with high purity He for 1 h. Pulses of 10% NO in He were injected every 0.5 h to determine the concentration of adsorbed NO on the sulfided catalyst. Evolved gases were detected by a Balzers mass spectrometer. The mixture ensured a pulse size of 7.5 μmol NO/pulse. Injections were repeated until adsorption was not longer detected. NO adsorption was calculated as the difference between the NO signal at a given pulse and an NO signal at which adsorption was not observed. The total concentration of NO adsorbed (μmol per 1 g catalyst) was calculated as the sum of the individual NO uptakes per pulse [24,25].

2.3. Kinetic test

Kinetic studies were carried out in a continuous flow fixed-bed reactor system. The stainless steel, glass-lined coated reactor was loaded with 0.05 g of catalyst, diluted in 1 g SiC, for each run, and the HDN reaction was performed at constant temperature, pressure, and feed composition. Gas and liquid feed were introduced to the reactor via high pressure mass flow meters (Bronkhorst) and a HPLC pump (Shimadzu LC-20AD), respectively. After separation of liquid and gas effluent phase, the liquid was collected via a 16 port sampling valve every 1.5 h. The liquid samples were analyzed by off-line gas chromatography with a HP 6890 GC instrument equipped with a flame ionization detector (FID) and 60-m-long DB-17 capillary column (Agilent, 0.25 mm i.d., 0.25-μm film thickness). The reproducibility of the measurements was ±5%.

Prior to the kinetic experiments, the catalysts were activated in situ in 10% H_2S in H_2 flow at 400 °C and 1.8 MPa for 8 h. After cooling to room temperature in the sulfiding agent, the catalysts were flushed with hydrogen and the liquid feed flow. The reaction

temperature was set to 370 °C and the total pressure to 5.0 MPa. The kinetic study was obtained from the samples taken after 16 h time on stream (TOS).

HDN was investigated as a function of space time. Space time was based on the OPA feed rate only and is defined as m_{cat}/F_{OPA}, where m_{cat} is the amount of the oxide catalyst precursor and F_{OPA} is the molar flow of OPA [(h)·(g of catalyst)/(mol of OPA)]. Reactions were performed in great excess of hydrogen, keeping the ratio of liquid and gas flow constant to ensure constant partial pressures. The H_2/HC value is 330 Ndm^3/dm^3, whereas the H_2/OPA molar ratio is approximately 220. The initial OPA partial pressure was 17.9 kPa in a mixture of hexadecane and tetradecane as a solvent. To study the effect of dibenzothiophene (DBT) on OPA HDN, feed with different DBT partial pressures were used: 0, 1.7, 3.4, and 5.1 kPa. To determine the hydrogenation to dehydrogenation ratio, ethylbenzene or ethylcyclohexane was added (4.4 kPa).

In order to better understand the impact of DBT on the OPA HDN carried out on NiMoS/γ-Al_2O_3, an independent set of experiments was performed at identical reaction conditions (T = 370 °C, p = 5.0 MPa) and the space time of 82 h g_{cat}/mol. After catalyst activation, as described previously, the reaction was performed applying the feed containing only 17.9 kPa OPA. After 16 h time on stream, the steady state was reached, and 3.4 kPa of DBT was cofed into the reactor. Finally, DBT was removed, after 6 h TOS, and the reaction was run for further 24 h in a feed containing only OPA. During the transient time, the product analysis was performed more frequently to ensure appropriate following of the concentration profile.

The stability of the NiMoS/γ-Al_2O_3 catalyst was studied to understand the deactivation when the OPA HDN is carried out in the absence of DBT. After activation, as described earlier, the catalyst was reduced under reaction conditions of temperature and pressure (370 °C and 5 MPa) in pure H_2 for 2, 6, and 10 h. Then, the liquid phase containing only OPA (17.9 kPa) was introduced into the reactor with the space time of 82 h g_{cat}/mol. The product analysis was performed every 5 min in the first hour and further on every hour.

The conversion of OPA to nitrogen-free products is referred to as the HDN conversion and is calculated according to the equation:

$$\text{OPA HDN conversion} = \frac{c_{[\text{OPA}]_0} - c_{[\text{OPA}]} - c_{[\text{N}]}}{c_{[\text{OPA}]_0}}$$

where $c_{[OPA]o}$ and $c_{[OPA]}$ are the OPA concentrations at time zero and at the measured space time and $c_{[N]}$ is the concentration of all nitrogen-containing intermediates at the measured space time. As nitrogen-containing intermediates were not detected, the OPA HDN conversion was equal to the total OPA conversion.

The determination of the OPA HDN reaction order was done using the integral method, applying appropriate concentration–space time dependency. The following power law model was used:

$$-r = \frac{dp_{[\text{OPA}]}}{dt} = k \cdot p^n_{[\text{OPA}]} \cdot p^m_{[\text{H2}]}$$

where r is the rate of the OPA HDN reaction, k the apparent rate constant, $p_{[OPA]}$ the partial pressure of OPA, $p_{[H2]}$ the partial pressure of hydrogen, t the space time based on OPA feed rate, n the reaction order in OPA, and m the reaction order in hydrogen. Considering that the reaction is carried out in great excess of hydrogen (H_2 partial pressure is considered constant), the rate expression can be simplified as:

$$-r = \frac{dp_{[\text{OPA}]}}{dt} = k' \cdot p^n_{[\text{OPA}]}$$

where k' is the apparent rate constant that includes the factor of the hydrogen partial pressure. Calculation of the rate constants for the proposed mechanism was carried out by the Berkeley Madonna 7.0 program using the Runge–Kutta integration method.

Temperature-dependent experiments were performed in absence and presence of 3.4 kPa DBT to determine the apparent energy of activation for the OPA HDN on unpromoted MoS_2/γ-Al_2O_3 and promoted NiMoS/γ-Al_2O_3 catalysts. The temperature range studied was from 330 to 390 °C with 20 °C step. The total pressure was 5 MPa, and the space time of 82 h g_{cat}/mol was chosen in order to obtain low OPA conversions. The apparent activation energies were calculated from a semilogarithmic plot of ln k' vs. $1/T$, using the Arrhenius equation:

$$\ln k' = \ln A - \frac{E_a}{RT}$$

where E_a is the apparent activation energy (kJ/mol), A is the pre-exponential factor, R is the molar gas constant (R = 8.314 J/(mol K)), and T is the absolute temperature (K).

3. Results

3.1. Catalyst characterization

3.1.1. Physicochemical properties

An overview of the physicochemical characteristics of the materials applied in this study is given in Table 1. The specific surface area of γ-Al_2O_3 support was 237 m^2/g. The Mo concentration in the oxide precursor was 8.6 wt.%, which corresponds to 2.5 Mo atoms/nm^2. The Ni concentration was 3.6 wt.% leading to a molar fraction of 0.4 Ni in the bimetallic catalyst precursor.

3.1.2. X-ray diffraction (XRD)

Oxidic catalyst precursors, Mo/γ-Al_2O_3 and NiMo/γ-Al_2O_3, did not show any additional diffraction reflections except the ones characteristic for the used support material (37, 39, 46, 61, and 67°2θ), Fig. S-1A and B in the Supplementary material. Thus, after molybdenum and nickel impregnation, new crystalline phases were not observed. The sulfided catalysts exhibited two diffraction peaks at around 33 and 59°2θ characteristic for the interplanar distances of 2.7 and 1.5 Å of the MoS_2 crystalline structure [26]. The diffraction peak at 14°2θ, characteristic for the (0 0 2) plane with interplanar distance of 6.1 Å, was not observed probably due to the low degree of stacking in the formed MoS_2 and NiMoS particles, Fig. S-1C and D in the Supplementary material.

3.1.3. Transmission electron microscopy (TEM)

Fig. S-2, in the Supplementary material, presents the TEM micrographs of the sulfided catalysts. The catalysts revealed the presence of typical layer like MoS_2 phase. The observed stacking did not exceed three layers confirming a good dispersion of the sulfide slabs on the γ-Al_2O_3 support as suggested by XRD.

3.1.4. Raman spectroscopy

The Raman spectra of the oxidic catalyst precursors are shown in Fig. S-3A in the Supplementary material. The Raman spectrum of Mo/γ-Al_2O_3 catalyst exhibits bands at 961, 860, 350, and 224 cm^{-1}. These vibrations are assigned to the stretching of terminal Mo═O, asymmetric stretching of bridging Mo-O-Mo, bending of terminal Mo═O, and deformation of bridging Mo—O—Mo bonds, respectively [27]. Due to the position of the highest frequency vibration and the presence of the characteristic bridging Mo—O—Mo bond vibration, it is proposed that the surface molybdenum species are present as polymolybdates [28]. After nickel impregnation, the Raman band corresponding to the terminal Mo═O symmetric stretching vibration was shifted downwards from 961 to 947 cm^{-1}. The shoulder at 860 cm^{-1} assigned to the

Table 1
Physicochemical properties of the γ-alumina support and the oxidic catalyst precursors.

Catalyst	Metal concentration wt.% (μmol/g)		Surface area (m^2/g)	Pore volume (cm^3/g)	Pore diameter (nm)
	Mo	Ni			
γ-Al_2O_3	–	–	237	0.75	8.5
Mo/γ-Al_2O_3	8.6 (895)	–	220	0.62	8.5
NiMo/γ-Al_2O_3	8.6 (895)	3.6 (610)	206	0.60	8.5

asymmetric stretching vibration of Mo—O—Mo bridging bond became more intense.

Raman spectra of the sulfided catalysts are given in Fig. S-3B in the Supplementary material. The bands related to the MoS_2 phase are found in both samples: 383 and 409 cm^{-1}, corresponding to Mo—S vibration along the basal plane and S—Mo—S vibration along the *c*-axis, respectively [29,30].

At the end of the stability test described in Section 3.6 (HDN of OPA in the absence of DBT), the used NiMoS/γ-Al_2O_3 catalyst was carefully washed with *n*-hexane and *i*-propanol, dried, and analyzed by means of Raman spectroscopy and elemental analysis. As shown in Fig. S-4 in the Supplementary material, the Raman spectrum of the used NiMoS/γ-Al_2O_3 catalyst exhibited bands at around 1240, 1440, 1570, and 1615 cm^{-1}. These weak bands can be related to polymeric aniline [31], suggesting the presence of N-containing coke. The precise assignment of the bands is difficult because the defined structure of the coke formed is not known; however, the elemental analysis of the used samples confirmed the presence of C and N in 1.93 and 0.16 wt.%, which corresponds to a C/N molar ratio of 14.

3.1.5. Temperature-programmed sulfidation (TPS)

The rate of sulfidation was followed by temperature-programmed reaction (10% H_2S in H_2) increasing the temperature by 5 °C/min. As previously established by Nag [32] and Arnoldy [33], the sulfidation mechanism is governed by oxygen for sulfur exchange reactions leading the oxide catalyst transformation through the oxy-sulfides to the fully sulfided species. The presence of three characteristic sections during sulfidation was common for the monometallic Mo/γ-Al_2O_3 and bimetallic NiMo/γ-Al_2O_3 catalyst (see Fig. S-5 in the Supplementary material).

In the first section, oxygen is exchanged for sulfur bonded to Mo^{6+}, as observed by H_2S consumption and parallel H_2O production. The temperature of the maximum H_2S consumption remained 120 °C for both Mo and NiMo/γ-Al_2O_3 catalysts. The second region is characteristic by the evolution of H_2S, which is paralleled/followed by H_2 consumption, which is used for the molybdenum reduction to Mo^{4+}. Introduction of Ni into the catalyst shifted the reduction temperature from 225 °C for the monometallic Mo/γ-Al_2O_3 catalyst to 205 °C for the bimetallic NiMo/γ-Al_2O_3 catalyst. The consumption of H_2S in the third section indicates further oxygen for sulfur exchange on Mo^{4+}, leading to the fully sulfided catalyst.

3.1.6. NO adsorption

NO preferentially adsorbs on coordinatively unsaturated metal cations at the edge sites of the sulfide particles [24]. Molybdenum Mo^{6+} cations do not adsorb NO strongly because they have a d^0 configuration, which does not allow the accommodation of the unpaired antibonding electron of NO [34–36]. The support material (γ-Al_2O_3) does not adsorb NO as well. Volumetric adsorption of NO has been widely used to correlate the catalyst activity with the concentration of the active sites or Co and Ni atoms in the MoS_2 phase [37–41]. The adsorption mode of NO molecules on Mo and Co(Ni) cations is still controversial. Mononitrosyl or dinitrosyl species and different adsorption mechanisms have been proposed with basis on IR spectroscopy, STM, and DFT calculations [34,42]. Thus, it is difficult to calculate the exact concentration of the active sites using NO adsorption. Nevertheless, the concentration of active sites calculated under the assumption of dinitrosyl species formation [38] is the lowest boundary.

As shown in Fig. S-6A and B, in Supplementary material, the intensity of the NO peaks increased more rapidly in the case of MoS_2/γ-Al_2O_3 than in the case of NiMoS/γ-Al_2O_3, indicating a larger concentration of active sites in the latter material. A slower uptake following an initial rapid one indicated that a subtle rearrangement is needed to accommodate all NO, Fig. S-6C, in Supplementary material. At steady state, further adsorption was not observed after the same number of pulses for both catalysts. The total NO uptake corresponded to 130 μmol/g_{cat} for the MoS_2/γ-Al_2O_3 and 160 μmol/g_{cat} for the NiMoS/γ-Al_2O_3 sulfide catalyst. Considering the stoichiometry of the dinitrosyl species, the concentration of the active sites is 65 μmol/g_{cat} for the MoS_2/γ-Al_2O_3 and 80 μmol/g_{cat} for the NiMoS/γ-Al_2O_3. Thus, the addition of 3.6 wt.% of Ni as a metal promoter enhanced the concentration of coordinatively unsaturated metal cations by about 25%.

3.2. Hydrodenitrogenation of o-propylaniline

The product yields as a function of the OPA conversion are presented in Figs. 1 and 2 in the absence and presence of DBT, respectively. Nitrogen-free products detected on both catalysts were propylbenzene (PB), propylcyclohexane (PCH), and three isomers of propylcyclohexene (PCHE): 1-propylcyclohexene, 3-propylcyclohexene, and propylidene cyclohexane. The yield of 1-propylcyclohexene was the highest, which is in line with its highest stability, suggesting that the isomers are equilibrated. Thus, for further analysis, all three isomers were lumped together.

PB (formed from OPA via direct C(sp^2)–N bond cleavage) with around 20% and PCH (formed as a secondary end product) together with PCHE with combined 12% were the main products detected in the absence and presence of DBT on MoS_2/γ-Al_2O_3. The intermediate product of HYD, propylcyclohexylamine (PCHA), was not detected on both catalysts. PCHE was the single intermediate observed.

Two additional reaction pathways were also examined, i.e., the hydrogenation of propylbenzene to propylcyclohexane and the reverse dehydrogenation of propylcyclohexane to propylbenzene. From the parallel reaction of o-propylaniline and ethylbenzene/ethylcyclohexane, it is concluded that hydrogenation and dehydrogenation of aromatic rings without basic nitrogen does not occur under our conditions or are very slow compared with the conversion of substituted propylbenzene. Conversion of ethylbenzene or ethylcyclohexane was not observed over the whole space time range. This is attributed to the strong competitive adsorption of molecules containing an amine functional group [11,43,44].

3.3. Kinetic modeling of the HDN OPA network

The HDN reaction was first order in OPA for MoS_2/γ-Al_2O_3 and NiMoS/γ-Al_2O_3 catalysts at all reaction conditions studied (in the presence and absence of DBT). Corresponding concentration–time

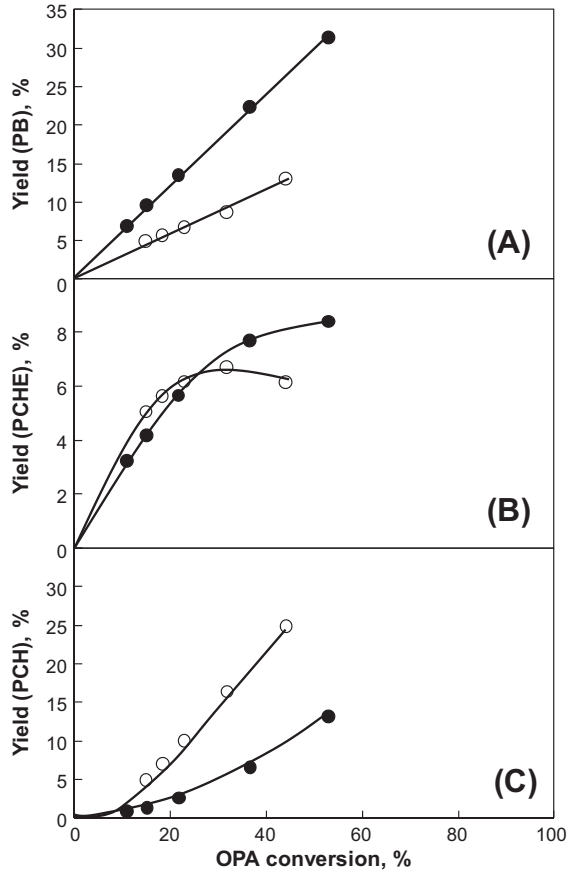

Fig. 1. Yield of propylbenzene (A), propylcyclohexene (B), and propylcyclohexane (C) as a function of o-propylaniline HDN conversion on MoS_2/γ-Al_2O_3 (●) and NiMoS/γ-Al_2O_3 (○) catalyst. The experiments were carried out in the absence of DBT.

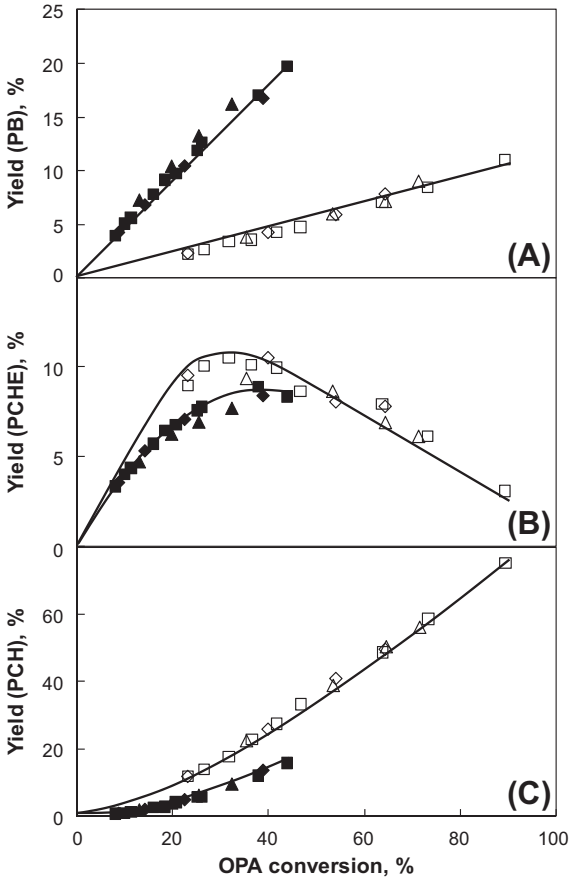

Fig. 2. Yield of propylbenzene (A), propylcyclohexene (B), and propylcyclohexane (C) as a function of OPA HDN conversion on MoS_2/γ-Al_2O_3 (▲, ■, ♦) and NiMoS/γ-Al_2O_3 (Δ, □, ◇) catalyst. The experiments were carried out in the presence of DBT. The following symbols are used for different DBT partial pressures: (▲, Δ) 1.7 kPa, (■, □) 3.4 kPa, (♦, ◇) 5.1 kPa.

profiles as presented in Fig. 3 show a linear correlation with the apparent rate constant as the slope.

Considering the proposed reaction network shown in Fig. 4, the following differential equations are obtained. Note that propylcyclohexene (PCHE) is considered as kinetic primary product, because propylcyclohexylamine (PCHA) was not observed.

$$\frac{dp_{[OPA]}}{dt} = -k'_1 \cdot p_{[OPA]} - k'_2 \cdot p_{[OPA]}$$

$$\frac{dp_{[PB]}}{dt} = k'_1 \cdot p_{[OPA]}$$

$$\frac{dp_{[PCHE]}}{dt} = k'_2 \cdot p_{[OPA]} - k'_3 \cdot p_{[PCHE]}$$

$$\frac{dp_{[PCH]}}{dt} = k'_3 \cdot p_{[PCHE]}$$

After data fitting, applying the Runge–Kutta integration method, rate constants were obtained in mol/h g_{cat} (see Table 2). Fitting results of the OPA HDN product distribution on MoS_2 and NiMoS/γ-Al_2O_3 catalysts in absence and presence of DBT are presented in supplementary material in Figs. S-7 and S-8, respectively.

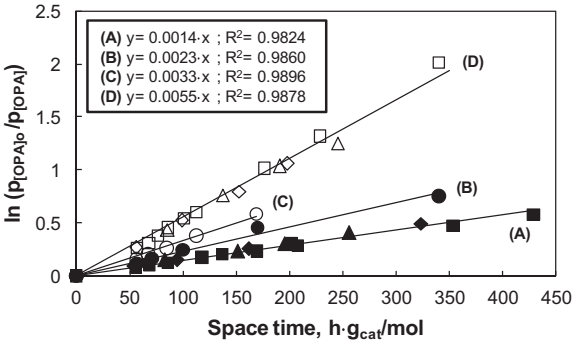

Fig. 3. Determination of the apparent rate constants (mol/h g_{cat}) for the first rate reaction of the o-propylaniline HDN carried out on MoS_2/γ-Al_2O_3 (●, ▲, ■, ♦) and NiMoS/γ-Al_2O_3 (○, Δ, □, ◇) catalyst. The following symbols are used for different DBT partial pressures: (●, ○) 0 kPa, (▲, Δ) 1.7 kPa, (■, □) 3.4 kPa, and (♦, ◇) 5.1 kPa. The reactions carried out in the presence of DBT are marked with (A) for MoS_2/γ-Al_2O_3 and (D) for NiMoS/γ-Al_2O_3, and in the absence of DBT are marked with (B) for MoS_2/γ-Al_2O_3 and (C) for NiMoS/γ-Al_2O_3 catalyst.

3.4. Influence of Ni substitutions on the o-propylaniline HDN

HDN conversion of OPA is equal to the total OPA conversion, because the only nitrogen-containing intermediate, PCHA, was not detected in the products. Both in the absence and in the presence of DBT, NiMoS/γ-Al_2O_3 was more active for nitrogen removal than MoS_2/γ-Al_2O_3, Fig. 3. With nickel promotion of MoS_2/γ-Al_2O_3 catalyst, the total apparent rate constant ($k' = k'_1 + k'_2$) increased from 2.3 to 3.3 mmol/h g_{cat} in sulfur-free conditions and from 1.5 to 5.3 mmol/h g_{cat} in the presence of DBT.

For a detailed analysis of how nickel influences the HDN network, the yield of individual products are presented as a function of space time in Fig. 5 for reactions carried out in absence and in

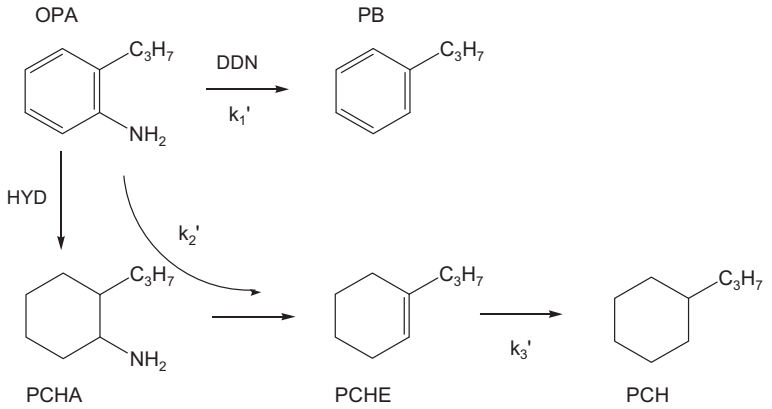

Fig. 4. Reaction network of the o-propylaniline HDN reaction with differentiation between the direct denitrogenation (DDN) and the hydrogenation (HYD) pathway.

Table 2
The rate constants (mol/h g_{cat}) obtained for the OPA HDN at 370 °C, 5 MPa on MoS_2 and $NiMoS/\gamma\text{-}Al_2O_3$ catalysts.

Catalyst	Feed	Rate constants (mol/h g_{cat})			
		k'	k'_1	k'_2	k'_3
$MoS_2/\gamma\text{-}Al_2O_3$	OPA	0.0023	0.0014	0.0009	0.0062
	OPA + DBT	0.0015	0.0007	0.0008	0.0060
$NiMoS/\gamma\text{-}Al_2O_3$	OPA	0.0033	0.0010	0.0023	0.0270
	OPA + DBT	0.0053	0.0006	0.0047	0.0312

the presence of 1.7, 3.4, and 5.1 kPa DBT. For all conditions studied, the yield of propylbenzene, the product of the DDN route, was higher for the unpromoted MoS_2 catalyst (see Fig. 5A,a and B,a). Promotion by Ni cations led to a decrease in the DDN rate by approximately 40% in absence and presence of DBT.

In contrast, the HYD rate was enhanced by Ni promotion, indicated by the higher yield of PCHE and PCH (see Fig. 5A,b, A,c, and B,b, B,c). In absence of DBT, the HYD rate was enhanced 2.5 times, and in the presence of DBT, the rate was approximately five times higher than for $MoS_2/\gamma\text{-}Al_2O_3$. As previously noted, the

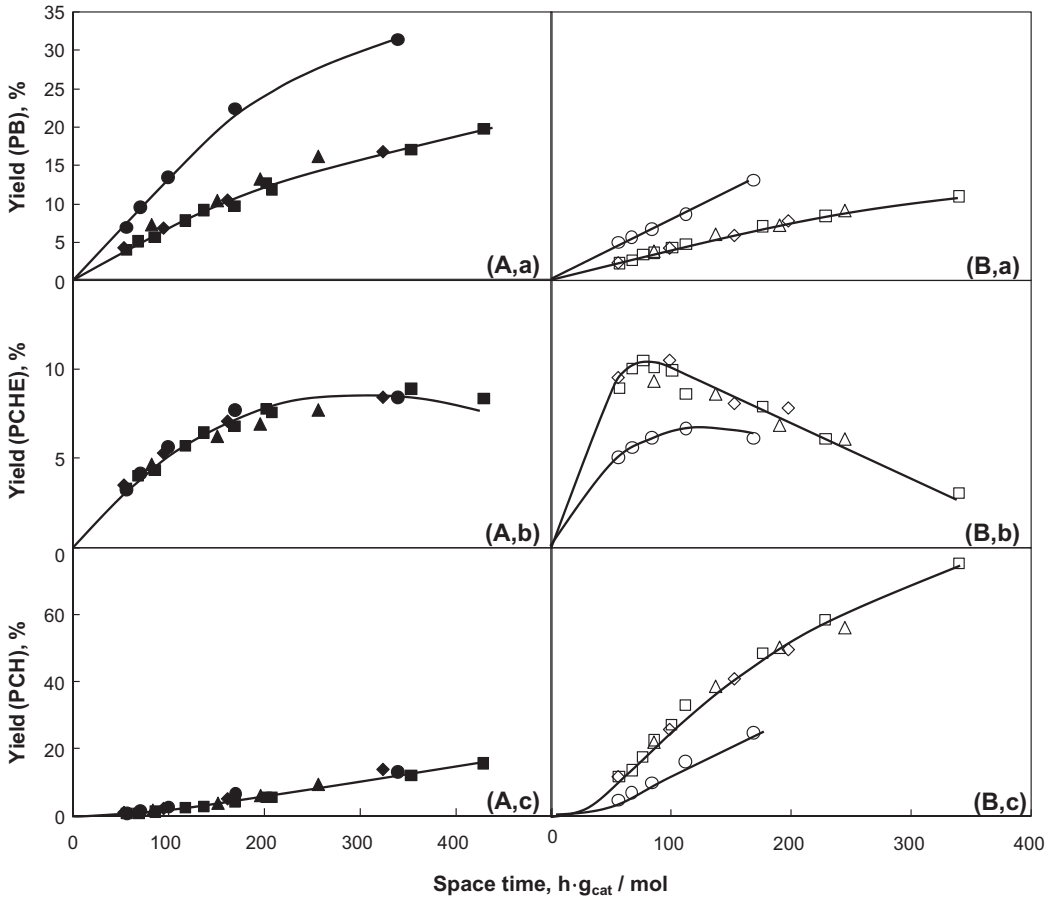

Fig. 5. Yield of propylbenzene (a), propylcyclohexene (b), and propylcyclohexane (c) as a function of space time on $MoS_2/\gamma\text{-}Al_2O_3$ (A) and $NiMoS/\gamma\text{-}Al_2O_3$ (B) catalyst. Diverse symbols are used for different DBT partial pressures: (●, ○) 0 kPa, (▲, △) 1.7 kPa, (■, □) 3.4 kPa, and (♦, ◇) 5.1 kPa.

Table 3
Yield of the OPA HDN products in the absence of DBT.

Catalyst	Space time (h g_{cat}/mol)	HDN conversion (%)	Yield (%)			(PCH + PCHE)/PB
			PB	PCHE	PCH	
MoS_2/γ-Al_2O_3	56	11.0	6.9	3.2	0.8	0.6
	169	36.6	22.4	7.7	6.5	0.7
NiMoS/γ-Al_2O_3	56	14.9	5.0	5.1	4.9	2.0
	169	44.1	13.1	6.1	24.9	2.4

Table 4
Yield of the OPA HDN products in the presence of 3.4 kPa DBT.

Catalyst	Space time (h g_{cat}/mol)	HDN conversion (%)	Yield (%)			(PCH + PCHE)/PB
			PB	PCHE	PCH	
MoS_2/γ-Al_2O_3	56	8.0	4.0	3.3	0.7	1.0
	353	37.9	17.0	8.9	12.0	1.2
NiMoS/γ-Al_2O_3	56	23.1	2.3	9.0	11.9	9.2
	176	63.8	7.1	7.9	48.7	8.0
	340	89.4	11.0	3.1	75.3	7.1

intermediate product of the OPA hydrogenation route (propylcyclohexylamine, PCHA) was not detected; therefore, (PCH + PCHE) to PB ratios are calculated in order to compare HYD to DDN rates. See Tables 3 and 4 for OPA HDN carried out in absence and presence of 3.4 kPa DBT, respectively.

3.5. Effect of dibenzothiophene (DBT) on the o-propylaniline HDN

The comparison between OPA HDN carried out in the absence and the presence of 1.7, 3.4, and 5.1 kPa DBT is given for MoS_2/γ-Al_2O_3 and NiMoS/γ-Al_2O_3 in Fig. 3. DBT reduces the rate of HDN on MoS_2/γ-Al_2O_3, while it increases the rate on NiMoS/γ-Al_2O_3. The apparent rate constant decreased from 2.3 to 1.5 mmol/h g_{cat} for the former, while it increased from 3.3 to 5.3 mmol/h g_{cat} for the latter. As soon as a small amount of DBT was present, the impact on the HDN rate was observed, and there were no further changes with increase in the DBT partial pressure.

To inspect more closely the influence of DBT, the yield of the individual products is displayed as a function of space time in Fig. 5A and B, for MoS_2/γ-Al_2O_3 and NiMoS/γ-Al_2O_3, respectively. In case of MoS_2/γ-Al_2O_3, the DDN rate was selectively reduced (see Fig. 5A,a). The HYD route remained in contrast unaffected (see Fig. 5A,b and A,c). Also with NiMoS/γ-Al_2O_3, the rate of the DDN was reduced by DBT (Fig. 5B,a). Interestingly, the HYD route was promoted, as seen by the increase in the yields of PCHE and PCH (see Fig. 5B,b and B,c). Thus, the overall effect of DBT on the OPA HDN rate is negative on the MoS_2/γ-Al_2O_3 catalyst, because of poisoning of the DDN route, while on NiMoS/γ-Al_2O_3, the reduction in the DDN rate is overcompensated by the higher HYD rate. Again, it should be emphasized that under the chosen operating conditions the variation in the concentration of DBT did not affect the rates effect on individual pathways.

The rate of the DDN route on the MoS_2/γ-Al_2O_3 catalyst was reduced by the addition of DBT, indicated by change in the rate constant (k_1') from 1.4 to 0.7 mmol/h g_{cat}. On NiMoS/γ-Al_2O_3, the rate constant of DDN route (k_1') decreased from 1.0 to 0.6 mmol/h g_{cat}. Thus, the presence of DBT reduced the DDN reaction route by approximately 50% for both catalysts. Interestingly, increasing partial pressures of DBT did not further reduce the rate of DDN. In the presence of DBT, the HYD rate on MoS_2/γ-Al_2O_3 was unaffected, while on NiMoS/γ-Al_2O_3, it doubled (see the PCHE + PCH yields in Tables 3 and 4 for the reaction carried out in absence and presence of 3.4 kPa DBT).

In addition, the hydrodesulfurization (HDS) of DBT during OPA HDN has been followed to monitor the preferred reaction pathway of sulfur removal. The DBT conversion over unpromoted MoS_2/γ-Al_2O_3 catalyst reached 50% at the highest OPA space time. In Fig. 6, DBT HDS product distribution is presented for both MoS_2/γ-Al_2O_3 (A) and NiMoS/γ-Al_2O_3 (B) catalysts. Biphenyl (BPh), the product of the direct desulfurization (DDS) route, was the main sulfur-free product in both cases, while the partly hydrogenated product, phenylcyclohexane (PhCH), is minority product. With increasing DBT conversion, the yield of PhCH increased linearly up to 7% and 15% on the Mo and NiMo catalyst, respectively. Note that the DBT conversion range is very different for the two

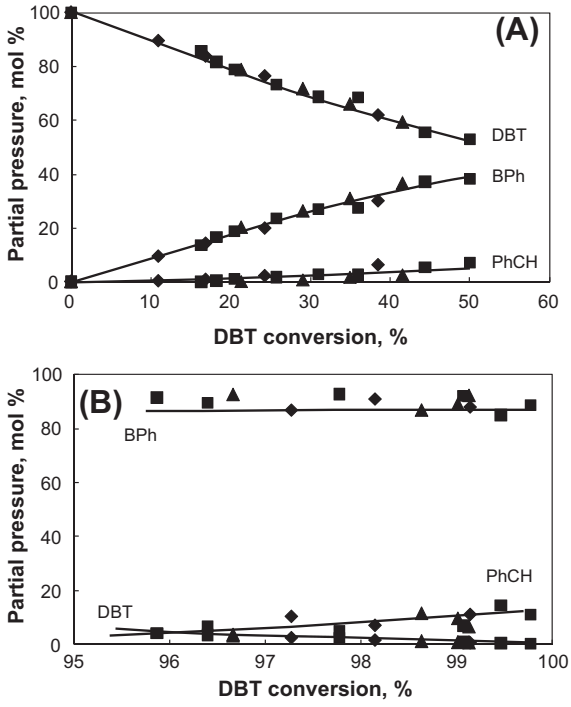

Fig. 6. The product distribution in HDS of dibenzothiophene (DBT) during HDN of o-propylaniline on MoS_2/γ-Al_2O_3 (A) and NiMoS/γ-Al_2O_3 (B) catalyst. The following symbols are used for different DBT partial pressures: (▲) 1.7 kPa, (■) 3.4 kPa, and (♦) 5.1 kPa.

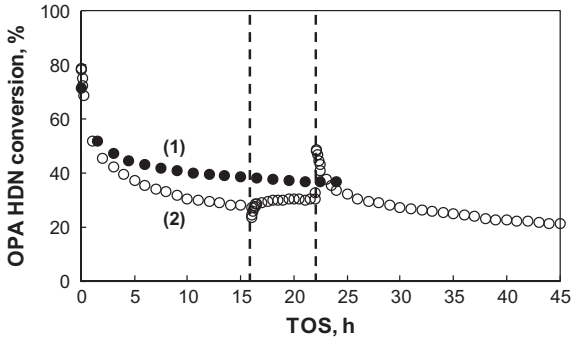

Fig. 7. OPA HDN conversion as a function of time on stream (TOS) for the reaction carried out on NiMoS/γ-Al_2O_3 catalyst. Steady state was reached after 16 h TOS in the: (1) presence of 3.4 kPa DBT and (2) absence of DBT. Experiment (2) was performed as a transient; 3.4 kPa DBT was cofed for 6 h after steady state was reached.

catalysts. However, the low concentration of PhCH and the absence of the fully hydrogenated HDS product bicyclohexyl on both catalysts suggest that the hydrogenation route of DBT is severely hindered by the presence of nitrogen-containing compounds.

Transient experiments with DBT were performed to better understand the impact of DBT on the OPA HDN, especially on the HYD route. The NiMoS/γ-Al_2O_3 catalyst was first stabilized for 16 h in pure OPA feed after which 3.4 kPa of DBT was cofed into the reactor for 6 h. Finally, DBT was removed. The OPA HDN conversion as a function of time on stream is shown in Fig. 7, and comparison was made with the reaction carried out from the beginning in the presence of 3.4 kPa of DBT. Stronger catalyst deactivation is observed, when the reaction is carried out in the absence of DBT. Further, it is confirmed that the OPA HDN conversion on NiMoS catalyst is higher in the presence (36.7%) than in absence of DBT (27.4%). After cofeeding DBT, at first, the OPA HDN conversion dropped (23.7%) and then slowly increased reaching slightly higher value (30.5%) than the value obtained after the first 16 h (27.4%). Nevertheless, the conversion never reached the value obtained when the reaction was run from the beginning in the presence of DBT. After removing DBT from the feed, the conversion swiftly increased (48.5%) and then gained a declining trend.

Attention must be paid on the yield of individual products to analyze the complex behavior in detail, see Fig. 8. The PB yield, as the only product of the DDN route, was higher in the absence (6.9%) than in the presence of DBT (3.5%). After cofeeding DBT, the PB yield dropped to the same level like when the reaction was run from the beginning in the presence of DBT. Removing DBT from the feed brought back the yield level to the previous value. The yield of PCHE, the only intermediate of the HYD route, was lower in absence (7.0%) than in the presence of DBT (9.7%). After cofeeding DBT, the PCHE yield increased to the same level as if the reaction was run from the beginning in the presence of DBT. Final removal of DBT from the feed depressed the yield again to the previous level. The yield of PCH, as the main end product from the HYD route, exhibited the same trend as the OPA HDN conversion, i.e., a negative effect caused by DBT cofeeding, followed by a positive yield recovery and finally followed by very positive effect once DBT was removed from the feed.

3.6. Stability of the NiMoS/γ-Al_2O_3 catalyst in the o-propylaniline HDN

Different hydrogen treatments were applied before HDN reactions to better understand the initial activity and deactivation on the NiMoS/γ-Al_2O_3 catalyst (in the absence of DBT). The highest initial OPA HDN conversion (78.5%) was observed when the catalyst was activated only by sulfidation (8 h at 400 °C in 1.8 MPa of 10% H_2S in H_2), Fig. 9. The initial conversion dropped when the catalyst sulfidation was followed by reduction at 370 °C in 5 MPa of H_2 for 2 h (65.0%), 6 h (55.5%), and it stayed almost constant after 10-h reduction (53.3%).

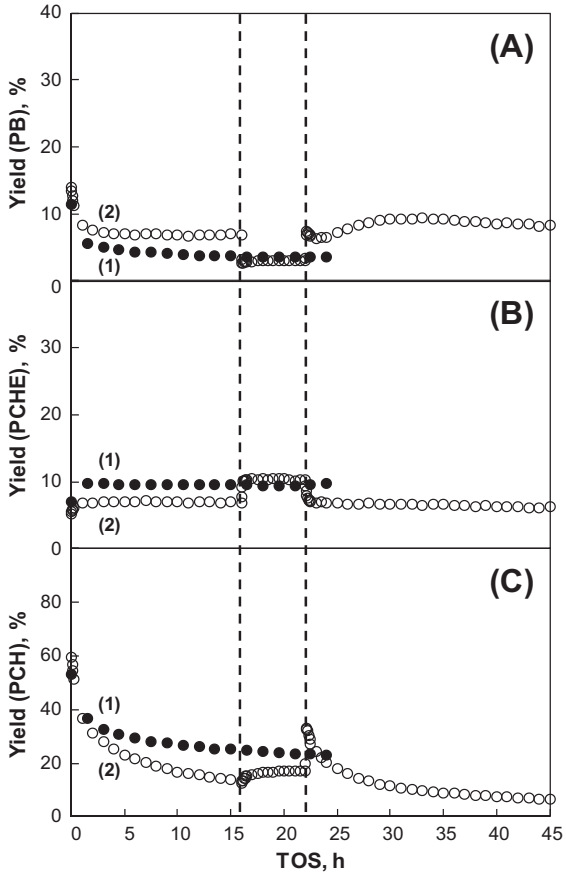

Fig. 8. Yield of propylbenzene (A), propylcyclohexene (B), and propylcyclohexane (C) as a function of time on stream for the reaction carried out on NiMoS/γ-Al_2O_3 catalyst. Steady state was reached after 16 h TOS in the: (1) presence of 3.4 kPa DBT and (2) absence of DBT. Experiment (2) was performed as a transient; 3.4 kPa DBT was cofed for 6 h after steady state was reached.

The product distribution as a function of the catalyst pretreatment is given in Fig. 10. The highest initial yield of PB and PCH

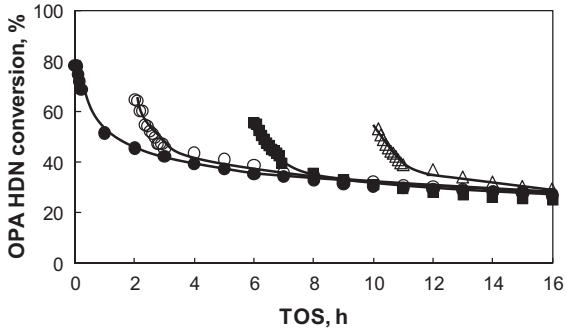

Fig. 9. OPA HDN conversion as a function of time on stream (TOS) for the reaction carried out on NiMoS/γ-Al_2O_3 catalyst in the absence of DBT. The following symbols are used for different catalyst pretreatments: (●) 8-h sulfidation in 10% H_2S in H_2 (400 °C, 1.8 MPa), (○) 8-h sulfidation in 10% H_2S in H_2 (400 °C, 1.8 MPa) followed by 2-h reduction in H_2 (370 °C, 5 MPa), (■) 8-h sulfidation in 10 % H_2S in H_2 (400 °C, 1.8 MPa) followed by 6-h reduction in H_2 (370 °C, 5 MPa), and (Δ) 8-h sulfidation in 10 % H_2S in H_2 (400 °C, 1.8 MPa) followed by 10-h reduction in H_2 (370 °C, 5 MPa).

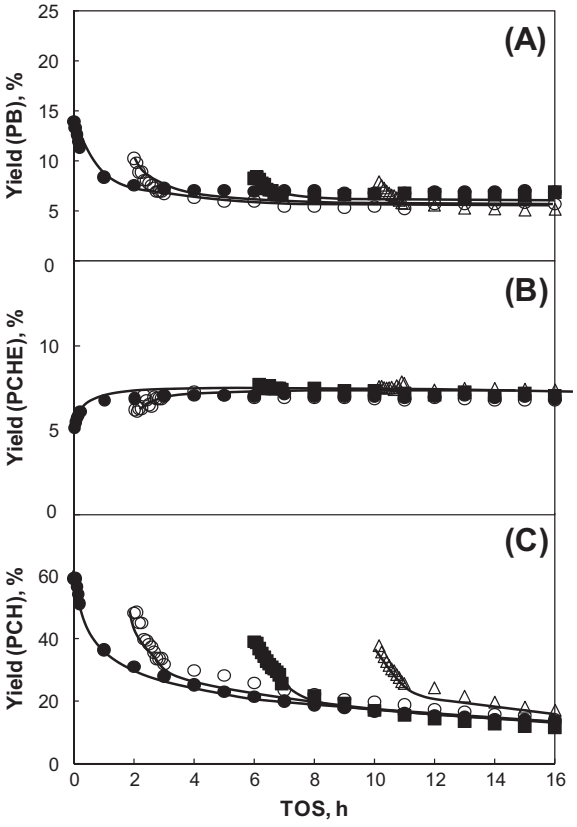

Fig. 10. Yield of propylbenzene (A), propylcyclohexene (B), and propylcyclohexane (C) as a function of time on stream (TOS) for the reaction carried out on NiMoS/γ-Al_2O_3 catalyst in the absence of DBT. The following symbols are used for different catalyst pretreatments: (●) 8-h sulfidation in 10% H_2S in H_2 (400 °C, 1.8 MPa), (○) 8-h sulfidation in 10% H_2S in H_2 (400 °C, 1.8 MPa) followed by 2-h reduction in H_2 (370 °C, 5 MPa), (■) 8-h sulfidation in 10 % H_2S in H_2 (400 °C, 1.8 MPa) followed by 6-h reduction in H_2 (370 °C, 5 MPa), and (Δ) 8-h sulfidation in 10 % H_2S in H_2 (400 °C, 1.8 MPa) followed by 10-h reduction in H_2 (370 °C, 5 MPa).

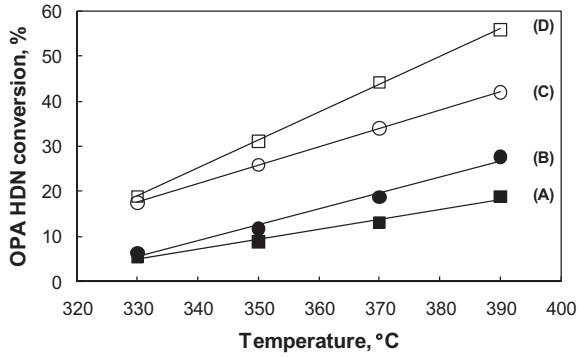

Fig. 11. OPA HDN conversion as a function of reaction temperature at the space time of 82 h g_{cat}/mol and total pressure of 5 MPa. The reactions carried out in the presence of 3.4 kPa DBT are marked with (A) for MoS_2/γ-Al_2O_3 and (D) for NiMoS/γ-Al_2O_3 and in the absence of DBT are marked with (B) for MoS_2/γ-Al_2O_3 and (C) for NiMoS/γ-Al_2O_3 catalyst.

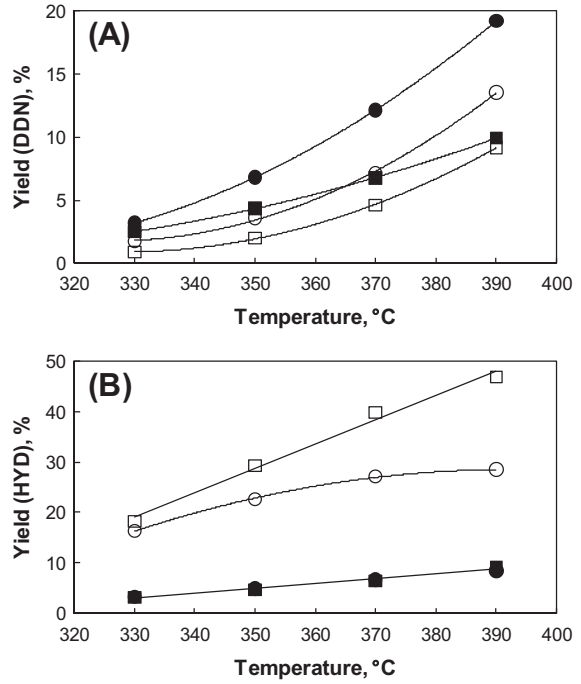

Fig. 12. Products yield of the two parallel reaction pathways: (A) direct denitrogenation and (B) hydrogenation as a function of temperature on MoS_2/γ-Al_2O_3 (●,■) and NiMoS/γ-Al_2O_3 (○, □) catalyst and at the space time of 82 h g_{cat}/mol and total pressure of 5 MPa. The following symbols are used for different DBT partial pressures: (●,○) 0 kPa and (■,□) 3.4 kPa.

was observed when the catalyst was only sulfided, 14.0% and 59.4%. When the reduction followed the activation, the PB and PCH yield decreased to 10.3% and 48.4% (2-h reduction), 8.3% and 39.3% (6-h reduction), and 8.0% and 37.7% (10-h reduction), respectively. The initial yield of PCHE increased from 5.1% (after catalyst sulfidation) to 6.2% (2-h reduction) reaching the final value of 8.1% (10-h reduction).

3.7. Temperature dependence of the catalytic reaction

The OPA HDN conversion for unpromoted MoS_2/γ-Al_2O_3 and promoted NiMoS/γ-Al_2O_3 catalysts as a function of reaction temperature is shown in Fig. 11, for the experiments performed in the presence and absence of DBT. For the studied temperature range (330–390 °C), in the presence of DBT, the OPA HDN conversion increased from 5.5% to 18.9% and from 18.9% to 55.9%, while in the absence of DBT, increased from 6.5% to 27.5% and from 17.5% to 41.9% for MoS_2/γ-Al_2O_3 and NiMoS/γ-Al_2O_3 catalyst, respectively.

To look more closely how the temperature influences the two parallel reaction routes, the yield of DDN (equal to PB yield) and HYD route products (equal to sum of PCHE and PCH yields) is shown in Fig. 12A and B, respectively. On both, MoS_2/γ-Al_2O_3 and NiMoS/γ-Al_2O_3 catalyst, poisoning of DDN route by DBT was more intense at higher temperature. The yield of HYD products on MoS_2/γ-Al_2O_3 catalyst was not affected by DBT over the whole range of temperature. On the contrary, on NiMoS/γ-Al_2O_3 catalyst, increase in yield was more pronounced at the higher temperatures. It is important to note that in the case of the OPA HDN reaction carried out in the absence of DBT on NiMoS/γ-Al_2O_3 catalyst, at 390 °C, certain activity decrease in the HYD route is observed.

The apparent activation energy for both catalysts was obtained from the Arrhenius equation using the semilogarithmic plot $\ln k'$ vs. $1/T$ plot, shown in Figs. 13 and 14, for the experiments performed in the presence and absence of DBT, respectively. In addition, the apparent activation energies for the two parallel routes were calculated based on the rate constants k'_1 for DDN and k'_2 HYD pathway. The corresponding rate constants were calculated (see Table 5) according to the first-order kinetics following the equations:

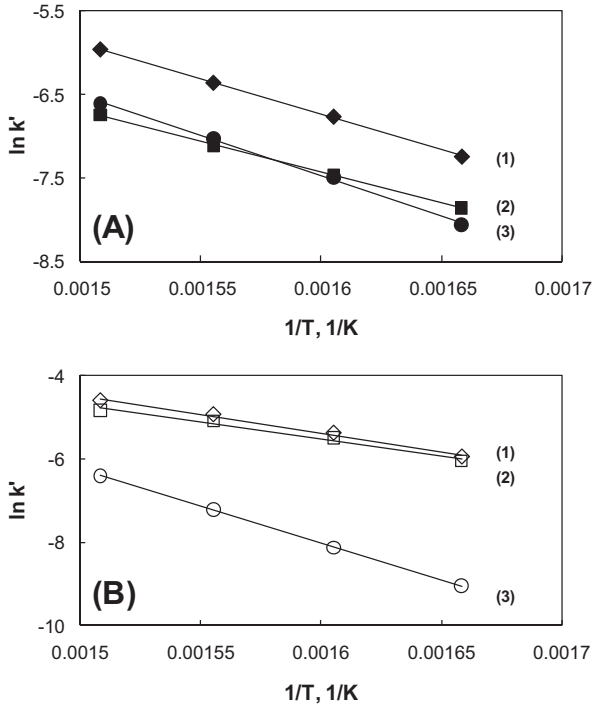

Fig. 13. The Arrhenius plot of the first-order apparent rate constants for the OPA HDN reaction, carried out in the presence of 3.4 kPa DBT on MoS_2/γ-Al_2O_3 (A) and NiMoS/γ-Al_2O_3 (B) catalyst and at the space time of 82 h g_{cat}/mol and total pressure of 5 MPa. The values are used for the determination of the total apparent activation energy (1) and apparent activation energies for the two parallel routes: HYD (2) and DDN (3).

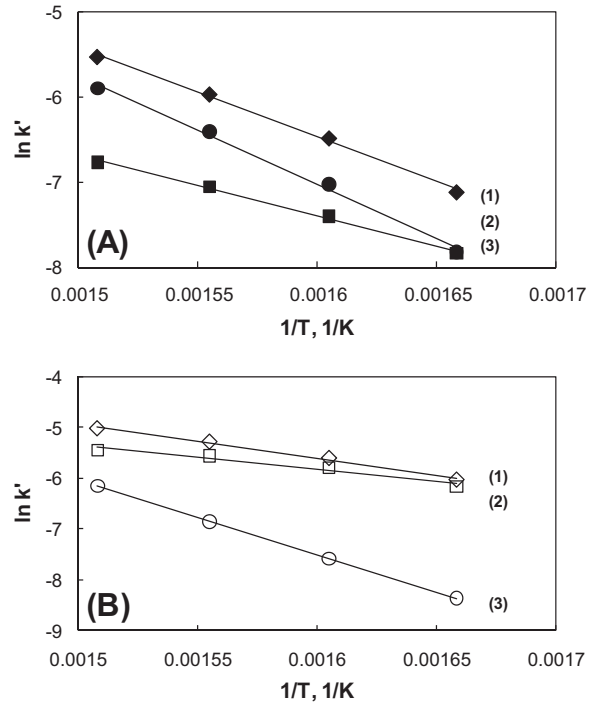

Fig. 14. The Arrhenius plot of the first-order apparent rate constants for the OPA HDN reaction, carried out in the absence of DBT on MoS_2/γ-Al_2O_3 (A) and NiMoS/γ-Al_2O_3 (B) catalyst. The values are used for the determination of the total apparent activation energy (1) and apparent activation energies for the two parallel routes: HYD (2) and DDN (3).

Table 5
The rate constants (mol/h g_{cat}) obtained for the OPA HDN at the space time t = 82 h g_{cat}/mol, p = 5 MPa on MoS_2 and NiMoS/γ-Al_2O_3 catalysts.

Feed	Catalyst	Temperature (°C)	Rate constants (mol/h g_{cat})		
			k'	k'_1	k'_2
OPA + DBT	MoS_2/γ-Al_2O_3	330	0.0007	0.0003	0.0004
		350	0.0012	0.0006	0.0006
		370	0.0015	0.0007	0.0008
		390	0.0026	0.0013	0.0013
	NiMoS/γ-Al_2O_3	330	0.0026	0.0001	0.0023
		350	0.0046	0.0003	0.0043
		370	0.0071	0.0007	0.0064
		390	0.0100	0.0016	0.0084
OPA	MoS_2/γ-Al_2O_3	330	0.0008	0.0004	0.0004
		350	0.0015	0.0009	0.0006
		370	0.0023	0.0014	0.0009
		390	0.0039	0.0027	0.0012
	NiMoS/γ-Al_2O_3	330	0.0024	0.0002	0.0022
		350	0.0037	0.0005	0.0032
		370	0.0051	0.0011	0.0040
		390	0.0066	0.0021	0.0045

$$k' = \frac{1}{t} \cdot \ln \frac{p_{[OPA]_0}}{p_{[OPA]}}$$

$$k' = k'_1 + k'_2$$

$$k'_1 = \frac{p_{[PB]} \cdot k'}{p_{[OPA]_0} \cdot [1 - e^{-k' \cdot t}]}$$

The values obtained for the apparent activation energy are listed in Table 6 for all conditions studied. In the presence of DBT, apparent activation energies of OPA HDN did not differ for the two catalysts, MoS_2/γ-Al_2O_3 (71 ± 1.8 kJ/mol) and NiMoS/γ-Al_2O_3 (75 ± 1.9 kJ/mol). In the absence of DBT, the apparent activation energy for MoS_2/γ-Al_2O_3 catalyst increased to 88 ± 2.2 kJ/mol. On the contrary, for NiMoS/γ-Al_2O_3 catalyst, it decreased to 56 ± 1.4 kJ/mol.

4. Discussion

The oxide catalyst precursors compared in this study have a Mo concentration of 2.5 Mo atoms/nm^2, which is below the monolayer concentration of approximately 4.6–5 atoms/nm^2 given for the γ-Al_2O_3 support [28,45]. XRD patterns of the oxide precursors do not exhibit reflections of Mo crystalline species, and the Raman spectra imply the existence of the polymolybdate species (see Figs. S-1 and S-3A in Supplementary material) [46,47]. Neither the presence of isolated MoO_4 tetrahedra nor crystalline MoO_3 was observed, due to the absence of the characteristic Raman bands at 896, 846, and 318 cm^{-1} and 996, 821, 667, and 377 cm^{-1} [48], respectively. Thus, the oxidic precursors are polymolybdates well dispersed on the γ-Al_2O_3 support. Sulfided catalysts, as shown in Raman spectra of Fig. S-3B, revealed the presence of the typical MoS_2 phase. In line with the characteristics of the oxide Mo species, the sulfide phase also exhibited high

Table 6
The apparent activation energy (kJ/mol) obtained for the OPA HDN, in the absence and presence of 3.4 kPa DBT, on MoS_2 and NiMoS/γ-Al_2O_3 catalysts.

Feed	Catalyst	Apparent activation energy (kJ/mol)		
		E_a	$E_{a\ (DDN)}$	$E_{a\ (HYD)}$
OPA + DBT	MoS_2/γ-Al_2O_3	71 ± 1.8	81 ± 2.0	61 ± 1.5
	NiMoS/γ-Al_2O_3	75 ± 1.9	147 ± 3.7	68 ± 1.7
OPA	MoS_2/γ-Al_2O_3	88 ± 2.2	106 ± 2.7	59 ± 1.5
	NiMoS/γ-Al_2O_3	56 ± 1.4	123 ± 3.0	40 ± 1.0

dispersion. The XRD pattern indicated low MoS_2 stacking degree with the absence of the diffraction peak at 14°2θ, Fig. S-1. TEM micrographs confirmed the high dispersion of the sulfided slabs with average MoS_2 stacking degree of two and slabs length below 10 nm on the γ-Al_2O_3 support (Fig. S-2). Furthermore, the formation of Ni sulfides was not observed (XRD and TEM).

The concentration of the accessible metal cations was 65 and 80 $\mu mol/g_{cat}$ for MoS_2/γ-Al_2O_3 and NiMoS/γ-Al_2O_3, respectively, indicating that the presence of Ni cations enhanced their concentration by approximately 25%. This is in line with the higher tendency of the lower valent cations in mixed sulfides to be accessible. It is interesting to note that this increase is considerably lower than the concentration of Ni added, suggesting the absence of NO specificity to exposed cations. We assume, therefore, for the following discussions that Ni incorporates only at the edges of the MoS_2 slabs, and the cations are exposed randomly.

Both materials showed a well-known profile with three sections during the reductive conversion (H_2S in H_2 mixture) from the supported oxide precursor to the final sulfide material. In the initial sulfiding section, low temperature sulfiding, oxygen is substituted by sulfur as seen in the marked consumption of H_2S followed by parallel H_2O production (not shown). H_2 is not consumed in this section (not shown). As previously published, the first Mo—S bond formation is leading to the conversion of oxides to different oxysulfidic species [33,49]. Cattaneo et al. published that the terminal Mo=O bonds, characteristic for the molybdenum monolayer species, are the first one to react forming Mo=S bonds [50]. XPS studies showed that at the low temperatures molybdenum reduces from Mo^{6+} to Mo^{5+} by oxidation of S^{2-} to bridging S_2^{2-} [51,52]. Further conversion above 150 °C shows that the sulfidation process is reversed, and for a short temperature interval, H_2S is released. The maximum of H_2S evolution between 205 °C and 225 °C is coupled with a maximum in H_2 consumption (not shown) indicating molybdenum reduction to Mo^{4+}. This reduction maximum is shifted from 225 °C for MoS_2/γ-Al_2O_3 to 205 °C in the presence of Ni cations. This indicates that incorporated Ni cations facilitate H_2 dissociation and so the overall catalyst reducibility. The subsequent consumption of H_2S, again followed by H_2O production, is concluded to be a high temperature sulfiding, related to full conversion of the precursor materials to the corresponding MoS_2 and NiMoS particles.

Under all reaction conditions and with all catalysts studied, the HDN of OPA follows two reaction pathways, which are summarized in Fig. 4. One involves the cleavage of the aromatic C(sp^2)—N bond and is assigned as the DDN, while the other involves the hydrogenation of the aromatic ring followed by nitrogen removal in form of NH_3 or substitution with an —SH group. That latter nitrogen removal is concluded to be so fast after the aromatic ring is hydrogenated that the intermediate propylcyclohexylamine has not been detected in the present experiments. In agreement with the literature, we conclude that the rate of the phenyl ring hydrogenation is limiting, while that of nitrogen removal is comparably large [53].

A question that must be addressed at this point is whether the nitrogen removal from the PCHA proceeds via Hofmann elimination or via nucleophilic substitution of NH_2 by an —SH group, followed by further C—S bond hydrogenolysis. The Hofmann-type elimination has been considered to be the main mechanism for nitrogen removal in the HDN of, e.g., cyclohexylamine and aniline-type compounds [54–57], when the reactions are carried out at the high temperature (350–370 °C) and pressure (3–5 MPa) and with H_2S partial pressure up to 17.5 kPa.

The other explanation, the S_N2 substitution of the NH_2 group with an —SH group, has been as well published [58,59]. For the first time, the thiol-type intermediates were obtained in the HDN reactions of *n*-hexylamines [60–63] carried out at the relatively low temperatures (270–320 °C) and pressure (3 MPa) and with high H_2S partial pressure (10–100 kPa). It was concluded that the selectivity to hexenes increases with lower and to thiols with higher H_2S partial pressure. Because of the relatively high reaction temperature and pressure (370 °C, 5 MPa) and the fact that the thiol-type compound was not identified (the carbon balance was fully closed under all reaction conditions), we can propose that the nitrogen removal after hydrogenation of the phenyl ring is governed by a Hofmann-type elimination of the aliphatic C(sp^3)—N bond.

Under the current reaction conditions, the products from the two pathways, DDN and HYD, are not interconnected, as Figs. 1A and 2A show a perfectly linear correlation to the overall conversion. This indicates that hydrogenation or dehydrogenation rates of the hydrocarbon products must be at least two orders of magnitude slower than the other reactions involved in the network. Because the reactions are first order in all reacting substrates, the question arises, whether this is a direct consequence of a slow true rate constant for the hydrogenation or of a very low adsorption constant. While we were unable to directly determine the adsorption constant, the high rate of the hydrogenation of the aromatic ring of o-propylaniline indicates that the low rate of hydrogenation of propylbenzene is related to a very low adsorption constant.

Intuitively, one would assume that the direct denitrogenation must be related to the presence of CUS, Lewis acid sites at the perimeter of the MoS_2 slabs. If this holds true, a higher concentration of such coordinatively unsaturated sites should enhance the rate of the DDN reaction. For the materials studied, that concentration of accessible Lewis acid sites was 25% higher for NiMoS/γ-Al_2O_3 than for MoS_2/γ-Al_2O_3.

Despite this higher concentration of coordinatively unsaturated sites on NiMoS/γ-Al_2O_3, the rate of DDN decreased drastically, in agreement with an earlier observation [64]. It is surprising that this decrease appears to be directly related to the relative concentration of accessible Mo cations at the perimeter of the MoS_2 slabs. Both samples, MoS_2/γ-Al_2O_3 and NiMoS/γ-Al_2O_3, contain identical concentration of Mo (895 $\mu mol/g_{cat}$). The additional Ni concentration added is 610 $\mu mol/g_{cat}$ leading to a mol fraction of 0.4 for Ni. The rate of DDN decreased with NiMoS/γ-Al_2O_3 to 60% of the value observed with MoS_2/γ-Al_2O_3. In parallel, the apparent energy of activation for the DDN route (in the presence of DBT) with NiMoS/γ-Al_2O_3 was almost twice higher than the one observed with MoS_2/γ-Al_2O_3 catalyst. It would be a remarkable coincidence, if the relative decrease in rate would be fortuitously identical to the nominal decrease in the average concentration of Mo available. Thus, we conclude that only Mo cations are associated with the active sites of the DDN pathway, i.e., that Ni cations are inactive. Note that we were not able to directly assess the relative concentration of Ni among the accessible cations. It should be emphasized, however, that the increase in the apparent activation energy indicates a slightly higher adsorption enthalpy for NiMoS/γ-Al_2O_3 catalyst.

It is also remarkable that this relative reduction induced by the presence of Ni cations (to 60%) also holds for the experiments in the presence of DBT, although the overall rate along that pathway decreased by about 50% in the presence of DBT. This decrease is attributed to the competitive adsorption of OPA and DBT on the accessible Lewis acid sites. Thus, all experimental evidence is in line with the conclusion that only accessible Mo cations participate in the DDN.

While the DDN of OPA is concluded to only occur on Mo cations, the analogous reaction of DBT desulfurization is not restricted. On MoS_2/γ-Al_2O_3 and NiMoS/γ-Al_2O_3, the dominating reaction pathway was the DDS leading to biphenyl as dominating product. The much higher rate of HDS with NiMoS/γ-Al_2O_3 than with MoS_2/γ-Al_2O_3 catalyst suggests that not only the concentration of CUS has increased but also the intrinsic rate constant of that reaction.

It has been established earlier that the sulfur vacancies as electron withdrawing sites are responsible for the DDS of DBT. Given that the DDS route requires DBT adsorption via sulfur σ-bonding, an analogous sorption mode of OPA is proposed, i.e., adsorption via σ-bonding of the amine nitrogen on the sulfur vacancy. DFT calculations for the sulfur edge also suggest that such vacancies are crucial for the sulfur removal. Besenbacher et al. [12] found that the C–S scission reaction has lower barriers at the S-edge than on the opposite Mo-edge. Consequently, it is suggested that the sites responsible for the DDN route in the OPA HDN are sulfur vacancies at the S-edge of the MoS_2 cluster with preferred adsorption via σ-bonding, Fig. 15C and lead to an overall mechanism via this route as proposed in Fig. 16.

Let us now turn to the second pathway, the reaction route relying on the hydrogenation of the aromatic ring. If accessible metal cations would be part of the active site, one would expect an increase in the rate proportional to the 25% increase in the concentration of CUS for NiMoS/γ-Al_2O_3 compared with MoS_2/γ-Al_2O_3. Therefore, the increase in the HYD rate (2.5 times when the reaction was carried out in absence of DBT) is twice as high as the rate that would be expected on the basis of the formation of new CUS sites for o-propylaniline adsorption. Thus, the higher HYD rate is attributed to an increase in the activity of the existing CUS sites or to a second more active site for hydrogenation. As the HYD rate is the first order in H_2 [65] and in OPA, the difference in the HYD rate can be caused by higher concentrations of adsorbed hydrogen and OPA or a higher intrinsic rate constant.

Many of speculations and suggestions have been put forward for this pathway. In essence, it is suggested that OPA adsorbs via the nitrogen atom of the amine group coordinating to a CUS site with the phenyl ring bends toward the electron-rich zone at the edge of the MoS_2 slab (“brim site”) showing a metal-like character [66–68]. DFT calculations imply that this edge acts as sites for the dissociative adsorption of hydrogen. Addition of Ni to the MoS_2/γ-Al_2O_3 catalyst increases the electron density of the brim sites [13,69], which would enhance the hydrogen dissociation on the catalyst surface needed for saturation of phenyl ring in OPA.

Having established that the presence of Ni cations in the MoS_2 layer induces a significantly higher rate in HYD of OPA by enhancing the electron density at the outer part of the basal plane of the sulfide slab, let us use the competitive HDS of DBT to better understand the nature and location of the sites for the HYD route for MoS_2/γ-Al_2O_3 and NiMoS/γ-Al_2O_3.

DBT induced neither promotion nor inhibition of the hydrogenation rate in the OPA HDN on MoS_2/γ-Al_2O_3 catalyst. As the presence of DBT must cause a reduction in the availability of the CUS sites at the rim by the adsorption of either DBT or H_2S, we conclude from the invariance of the rates that the sites for the hydrogenation and, hence, for the adsorption must be different from the CUS sites at the edge of the MoS_2 slab. In consequence, and in the absence of a fortuitous compensation, the equal rate allows us to conclude that the sites at the rim of MoS_2 are hardly involved in the HYD of OPA. This is in stark contrast to the suggestion of Sun et al. [66], indicating that the amine nitrogen does not interact with the accessible metal cations and would indicate also that the actual NH_3 elimination occurs on the brim sites. If OPA adsorbs on the brim zone, it would suggest that the interaction with the aromatic ring and the propyl group must outweigh the direct bonding of the amine nitrogen to Mo or Ni cations. The elimination of ammonia is concluded to occur via Hofmann-type elimination catalyzed by weak Brønsted acid sites available on the edge of the MoS_2 slabs in the presence of hydrogen. With respect to the reaction temperature, this proposal is well in line with the ammonia elimination from larger aliphatic amines observed during amine synthesis on zeolites [70].

DBT enhanced the HYD rate by a factor of five on NiMoS/γ-Al_2O_3. The positive influence was observed already at the lowest DBT partial pressure, but increase in the DBT partial pressure did not further affect the HYD rate. On the level of individual products, only PCH is affected by the long-term deactivation, Fig. 8C. Surprisingly, PB and PCHE were quite stable over the TOS, Fig. 8A and B. Besides the competitive adsorption of DBT and OPA on the sites responsible for the DDN route, competition was observed as well on the sites responsible for the HYD route. After the DBT removal, the yield of PCH drastically increased, Fig. 8C. Generally, the presence of DBT retarded the catalyst deactivation caused partially by reduction, as suggested by the results obtained after different hydrogen pretreatments, Figs. 9 and 10. The initial OPA HDN conversion, observed when the catalyst sulfidation was followed by reduction, 65.0% after 2-h reduction,

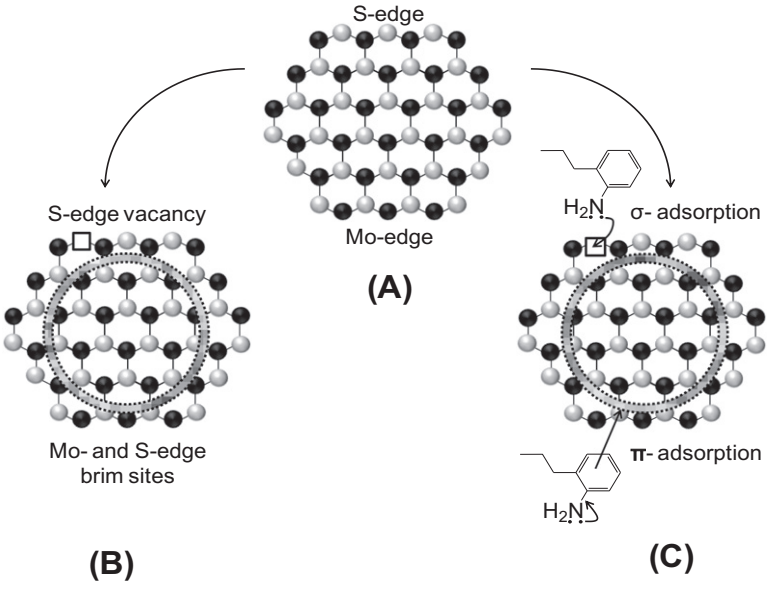

Fig. 15. Schematic presentation of MoS_2 structure: (A) differentiation between Mo- and S-edge; (B) different active sites: S-edge vacancies and Mo- and S-edge brim sites; (C) preferred adsorption modes of o-propylaniline depending on the available active sites, where Mo atoms are black and S atoms gray colored.

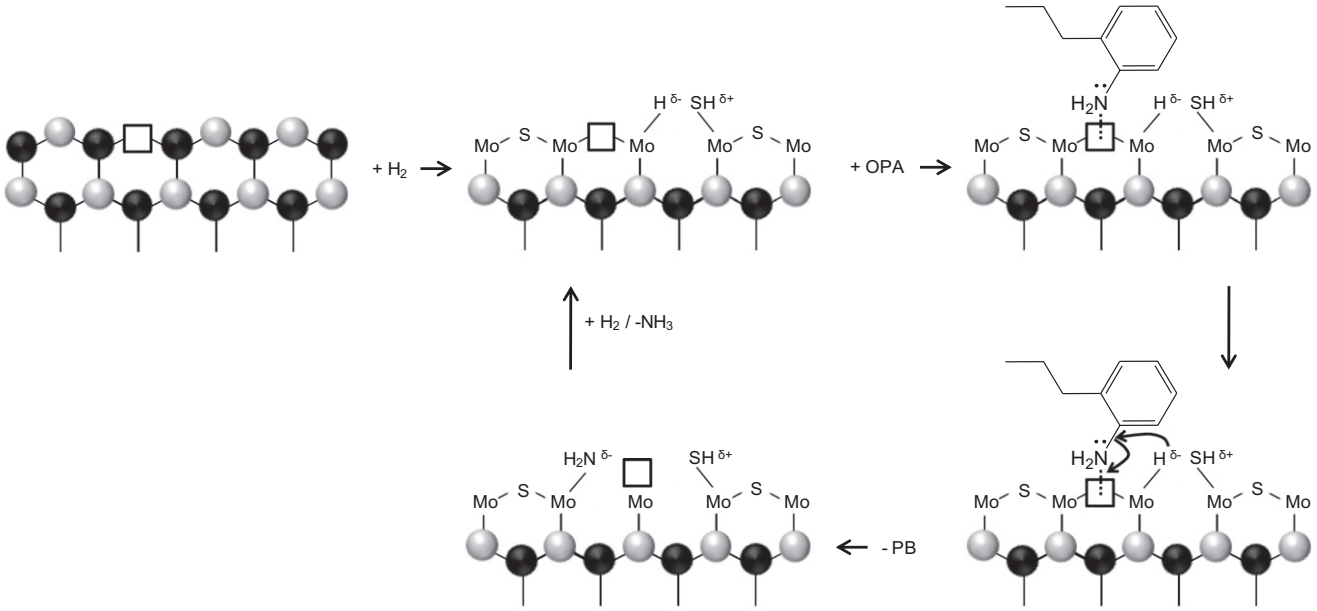

Fig. 16. Proposed mechanism of the o-propylaniline direct denitrogenation (DDN) on the S-edge of MoS_2 surface in sulfur-free conditions, where Mo atoms are black and S atoms gray on the colored.

55.5% after 6-h reduction, and 53.3% after 10-h reduction, was higher than the OPA HDN conversion at the corresponding TOS, observed when the catalyst was only sulfided, 45.0% after 2 h TOS, 35.0% after 6 h TOS, and 31.4% after 10 h TOS. Besides the catalyst deactivation by reduction, there is a second effect that induces very fast initial deactivation, 20% in all conditions studied, that occurs within the first hour after which the common activity level is reached, Fig. 9. The decrease in activity is attributed to the formation of coke from OPA as suggested by the Raman characterization and elemental analysis of the used catalyst. This is supported by the well-known fact that N-containing basic compounds are good coke precursors [71]. Furthermore, the polymerization of the reactant during the HDN process is well documented, and the structure of some dimers and trimers has been solved [72,73]. The rapid decrease in activity is also in line with the quick buildup of coke as soon as the reactant is introduced, as reported in [74]. The hindering of coke formation in the presence of DBT is assigned to the competitive adsorption of DBT or BPh, which decreases the concentration of OPA in the surface and thus decreases the presence of polymers. Moreover, the higher impact on the hydrogenation pathway implies that the formation of coke is favored on hydrogenation sites.

The promotion of the HYD route by the sulfur-containing compound is in contrast to the work previously published where the hydrogenation of OPA and 2,6-dimethylaniline was inhibited by the presence of H_2S [53,75]. However, one must notice that in those studies, H_2S was directly introduced in the feed or generated from dimethyldisulfide, while in the present study, the effect of DBT is followed. The conversion of DBT, which was very selective to BPh (Fig. 6), leads to a high concentration of H_2S in the system; thus, one might anticipate the same effect. However, as it is seen from our results, it is certainly not true, and thus, the effect of sulfur compounds in the feed is more complex than expected. The difference can be attributed to the mechanisms of interaction between the different sulfur-containing compounds and the catalyst surface. Both DBT and H_2S adsorb on CUS via σ-bonding of the sulfur atom. When H_2S is adsorbed, one can only imagine the creation of –SH groups, which increases the acidity of the surface. In contrast, the DDS of DBT leads to BPh desorption and S^{2-} ions instead of CUS. Moreover, DBT and BPh, as polyfunctional Lewis bases, can also donate π-electrons from the aromatic rings. Hence, DBT and the products of the HDS process modify the electronic environment in the vicinity of CUS and brim sites in a rather different manner than H_2S. Thus, it is reasonable to propose that the interaction of DBT and BPh with the metal cations (CUS) enhances the basicity of the surface, i.e., the electronic density of the brim sites.

Thus, it is remarkable that the higher concentration of accessible Ni cations at the rim of the NiMoS particles induces such a dramatic electronic effect that leads to a markedly higher hydrogenation rate. Scanning tunneling microscopy (STM) and DFT calculations suggest a significantly higher electron density in the NiMoS phase that is close to the edge of the sulfide slabs [12]. In the absence of specific DFT calculations on these sites, we would like to speculate that the intrinsically high electron density at these sites facilitates dissociative hydrogen adsorption and hydrogenation and that the presence of the polyfunctional Lewis bases such as DBT increases this electron density further or extends the electron-rich metallic-like zone.

5. Conclusion

The partial substitution of Ni cations in MoS_2 slabs of MoS_2/γ-Al_2O_3 increases the reducibility in the sulfidation procedure as well as the concentration of accessible metal cations in NiMoS/γ-Al_2O_3. The catalytic hydroconversion of o-propylaniline occurs via two reaction routes that have been shown unequivocally to occur on two separate sites.

The first reaction pathway, under our experimental conditions the direct elimination of NH_3 from o-propylaniline (DDN route), is catalyzed by accessible Mo cations. The presence of Ni cations dilutes these sites and leads to a reduction in the reaction rate along this pathway. It is interesting to note that the reduction in activity fits well to the statistical incorporation of Ni into MoS_2. If DBT is converted in parallel to o-propylaniline, its competitive adsorption reduces the DDN reaction rate by 50%. The identical relative reduction in the DDN rate by DBT for MoS_2/γ-Al_2O_3 and NiMoS/γ-Al_2O_3

is a strong indirect proof that the nature of these sites is identical in both catalysts.

The second reaction pathway, the hydrogenation of the aromatic ring with the subsequent elimination of NH_3 from o-propylcyclohexylamine (HYD route), is catalyzed only by brim sites. This is concluded from the absence of a negative effect of the parallel conversion of DBT on the hydroconversion of o-propylaniline on MoS_2/γ-Al_2O_3 and the dramatic enhancement of the rate for Ni-MoS/γ-Al_2O_3. If accessible metal cations would be involved in the adsorption site or the active site for the reaction, the presence of DBT should lead to a decrease in the reaction rate, because of the competitive adsorption of DBT. Using the argumentation from STM model studies, we suggest that the higher intrinsic rate is related to the higher electron density at the brim sites in the presence of Ni. It is remarkable that the presence of sulfur compounds enhance this in a dramatic way.

The present contribution shows, therefore, that the local manipulation of the substitution in MoS_2 structures and subtle promotion by coreactants could drastically enhance the hydrogenation ability of supported sulfides enhancing so their ability to hydroconvert heavy feeds.

Acknowledgments

This work was supported by Chevron Energy Technology Company. The authors would like to thank Dr. Alexander Kuperman and Dr. Axel Brait for fruitful discussions. The authors are also indebted to Prof. Roel Prins for discussion on the topic of hydrodenitrogenation.

Appendix A. Supplementary material

Supplementary data associated with this article can be found, in the online version, at doi:10.1016/j.jcat.2011.05.017.

References

[1] T.C. Ho, Catal. Rev. – Sci. Eng. 30 (1998) 117.
[2] F. Besenbacher, M. Brorson, B.S. Clausen, S. Helveg, B. Hinnemann, J. Kibsgaard, J.V. Lauritsen, P.G. Moses, J.K. Nørskov, H. Topsøe, Catal. Today 130 (2008) 86.
[3] R. Prins, V.H.J. de Beer, G.A. Somorjai, Catal. Rev. – Sci. Eng. 31 (1989) 1.
[4] P. Raybaud, Appl. Cat. A 322 (2007) 76.
[5] M. Sun, A.E. Nelson, J. Adjaye, J. Catal. 226 (2004) 32.
[6] E. Krebs, B. Silvi, P. Raybaud, Catal. Today 130 (2008) 160.
[7] L.S. Byskov, J.K. Nørskov, B.S. Clausen, H. Topsøe, Sulphur bonding in transition metal sulphides and MoS_2 based structures, in: T. Weber, R. Prins, R.A. van Santen (Eds.), Transition Metal Sulphides – Chemistry and Catalysis, Kluwer Academic Publishers, 1998.
[8] H. Topsøe, Appl. Catal. A 322 (2007) 3.
[9] J. Kibsgaard, A. Tuxen, K.G. Knudsen, M. Brorson, H. Topsøe, E. Laegsgaard, J.V. Lauritsen, F. Besenbacher, J. Catal. 272 (2010) 195.
[10] M. Sun, J. Adjaye, A.E. Nelson, Appl. Catal. A 263 (2004) 131.
[11] C. Moreau, J. Joffre, C. Saenz, P. Geneste, J. Catal. 122 (1990) 448.
[12] F. Besenbacher, M. Brorson, B.S. Clausen, S. Helveg, B. Hinnemann, J. Kibsgaard, J.V. Lauritsen, P.G. Moses, J.K. Nørskov, H. Topsøe, Catal. Today 130 (2008) 86.
[13] T.C. Ho, L. Qiao, J. Catal. 269 (2010) 291.
[14] S.H. Yang, C.N. Satterfield, J. Catal. 81 (1983) 168.
[15] H.A. Rangwala, I.G. Dalla Lana, F.D. Otto, H. Yeniova, K. Al-Nuaimi, Energy Fuels 4 (1990) 599.
[16] S. Eijsbouts, C. Sudhakar, V.H.J. de Beer, R. Prins, J. Catal. 127 (1991) 605.
[17] S. Eijsbouts, V.H.J. de Beer, R. Prins, J. Catal. 127 (1991) 619.
[18] L. Viver, V. Dominguez, G. Perot, S. Kasztelan, J. Mol. Catal. 67 (1991) 267.
[19] J.L. Lemberton, N. Gnofam, G. Perot, Appl. Catal. A 90 (1992) 175.
[20] R. Prins, M. Jian, M. Flechsenhar, Polyhedron 16 (1997) 3235.
[21] R.Z. Lee, M. Zhang, F.T.T. Ng, Top. Catal. 37 (2006) 121.
[22] X. Li, A. Wang, M. Egorova, R. Prins, J. Catal. 250 (2007) 283.
[23] B.S. Clausen, H. Topsøe, R. Candla, J. Villadsen, B. Lengeler, J. Als-Nielsen, F. Christensen, J. Phys. Chem. 85 (1981) 3868.
[24] Y. Okamoto, K. Ochiai, M. Kawano, K. Kobayashi, T. Kubota, Appl. Catal. A 226 (2002) 115.
[25] A.N. Desikan, L. Huang, S.T. Oyama, J. Phys. Chem. 95 (1991) 10050.
[26] R.W.G. Wyckoff, Crystal Structures, vol. 1, second ed., Interscience Publishers, New York, 1963, p. 280.
[27] G. Mestl, T.K.K. Srinivasan, Catal. Rev. Sci. Eng. 40 (1998) 451.
[28] I.E. Wachs, Catal. Today 27 (1996) 437.
[29] J.L. Verble, T.J. Wieting, Phys. Rev. Lett. 25 (1970) 362.
[30] T.J. Wieting, J.L. Verble, Phys. Rev. B 3 (1971) 4286.
[31] G.M. do Nascimento, T.B. Silva, P. Corio, M.S. Dresselhaus, J. Raman Spectrosc. 41 (2010) 1587.
[32] N.K. Nag, D. Fraenkel, J.A. Moulijn, B.C. Gates, J. Catal. 66 (1980) 162.
[33] P. Arnoldy, J.A.M. van den Heijkant, G.D. de Bok, J.A. Moulijn, J. Catal. 92 (1985) 35.
[34] F. Mauge, J. Lamotte, N.S. Nesterenko, O. Manoilova, A.A. Tsyganenko, Catal. Today 70 (2001) 271.
[35] N.-Y. Topsøe, H. Topsøe, Bull. Soc. Chim. Belg. 90 (1981) 1311.
[36] N.-Y. Topsøe, H. Topsøe, J. Catal. 75 (1982) 354.
[37] Y. Okamoto, A. Maezawa, T. Imanaka, J. Catal. 120 (1989) 29.
[38] N. Koizumi, S. Jung, Y. Hamabe, H. Suzuki, M. Yamada, Catal. Lett. 135 (2010) 175.
[39] N.-Y. Topsøe, H. Topsøe, J. Catal. 77 (1982) 293.
[40] N.-Y. Topsøe, H. Topsøe, J. Catal. 84 (1983) 386.
[41] N.-Y. Topsøe, H. Topsøe, O. Sørensen, B.S. Clausen, R. Candia, Bull. Soc. Chim. Belg. 93 (1984) 727.
[42] N.-Y. Topsøe, A. Tuxen, B. Hinnemann, J.V. Lauritsen, K.G. Knudsen, F. besenbacher, H. Topsøe, J. Catal. 279 (2011) 337.
[43] B.S. Gevert, J.-E. Otterstedt, F.E. Massoth, Appl. Catal. 31 (1987) 119.
[44] R. Prins, Adv. Catal. 46 (2001) 399.
[45] X. Wang, B. Zhao, D. Jiang, Y. Xie, Appl. Catal. A 188 (1999) 201.
[46] J. Medema, C. van Stam, V.H.J. de Beer, A.J.A. Konings, D.C. Koningsberger, J. Catal. 53 (1978) 386.
[47] C.P. Cheng, G.L. Schrader, J. Catal. 60 (1979) 276.
[48] J. Leyrer, M.I. Zaki, H. Knözinger, J. Phys. Chem. 90 (1986) 4775.
[49] P. Zeuthen, P. Blom, B. Muegge, F.E. Massoth, Appl. Catal. 68 (1991) 117.
[50] R. Cattaneo, T. Weber, T. Shido, R. Prins, J. Catal. 191 (2000) 225.
[51] J.C. Muijsers, T. Weber, R.M. van Hardeveld, H.W. Zandbergen, J.W. Niemantsverdriet, J. Catal. 157 (1995) 698.
[52] T. Weber, J.C. Muijsers, J.H.M.C. van Wolput, C.P.J. Verhagen, J.W. Niemantsverdriet, J. Phys. Chem. 100 (1996) 14144.
[53] M. Jian, R. Prins, Catal. Today 30 (1996) 127.
[54] M. Sun, R. Prins, J. Catal. 201 (2001) 138.
[55] L. Qu, R. Prins, J. Catal. 210 (2002) 183.
[56] P. Clark, X. Wang, P. Deck, S.T. Oyama, J. Catal. 210 (2002) 116.
[57] L. Qu, M. Flechsenhar, R. Prins, J. Catal. 217 (2003) 284.
[58] F. Rota, R. Prins, Top. Catal. 11/12 (2000) 327.
[59] L. Qu, R. Prins, Appl. Catal. A 250 (2003) 105.
[60] Y. Zhao, P. Kukula, R. Prins, J. Catal. 221 (2004) 441.
[61] Y. Zhao, R. Prins, J. Catal. 229 (2005) 213.
[62] R. Prins, Y. Zhao, N. Sivasankar, P. Kukula, J. Catal. 234 (2005) 509.
[63] R. Prins, M. Egorova, A. Röthlisberger, Y. Zhao, N. Sivasankar, P. Kukula, Catal. Today 111 (2006) 84.
[64] K. Shanthi, C.N. Pillai, J.C. Kuriacose, Appl. Cat. 46 (1989) 241.
[65] R.T. Hanlon, Energy Fuels 1 (1987) 424.
[66] M. Sun, A.E. Nelson, J. Adjaye, Catal. Lett. 109 (2006) 133.
[67] T.F. Jaramillo, K.P. Jørgensen, J. Bonde, J.H. Nielsen, S. Horch, I. Chorkendorff, Science 317 (2007) 100.
[68] B. Hinnemann, P.G. Moses, J. Bonde, K.P. Jørgensen, J.H. Nielsen, S. Horch, I. Chorkendorff, J.K. Nørskov, J. Am. Chem. Soc. 127 (2005) 5308.
[69] H. Topsøe, B.S. Clausen, N.-Y. Topsøe, E. Pedersen, W. Niemann, A. Müller, H. Bögge, B. Lengeler, J. Chem. Soc., Faraday Trans. I 83 (1987) 2157.
[70] V. Veefkind, J.A. Lercher, J. Catal. 180 (1998) 258.
[71] E. Furimsky, F. Massoth, Catal. Rev. 47 (2005) 297.
[72] G.C. Hadjiloizou, J.B. Butt, J.S. Dranoff, J. Catal. 135 (1992) 27.
[73] F.E. Massoth, S.C. Kim, Catal. Lett. 57 (1999) 129.
[74] M. Marafi, A. Stanislaus, Appl. Catal. A 159 (1997) 259.
[75] J. Van Gestel, C. Dujardin, J.C. Duchet, J. Catal. 202 (2001) 78.